

# Density Functional Theory Studies of Ruthenium Dye (N3) Adsorbed on a TiO<sub>2</sub> Brookite Cluster for Application in Dye Sensitized Solar Cells



I. F. Elegbeleye, N. E. Maluta and R. R. Maphanga

**Abstract** Titanium dioxide has been a subject of increasing interest due to its application in pigments, photocatalysis and semiconductor materials in dye sensitized solar cells (DSSC). Recent studies suggest that TiO<sub>2</sub> brookite exhibits good photocatalytic properties. Efficiency in excess of 11% has been achieved with the use of ruthenium (N3) dyes as DSSC sensitizer. The optical properties, energy level alignment and electronic state energy of the ruthenium (N3) sensitizer to TiO<sub>2</sub> cluster were studied to gain insight into the electron injection kinetics and electron injection efficiency of the dye/TiO<sub>2</sub> complex. The simulated absorption spectra show absorption peaks at 311, 388 and 480 nm. The HOMO of (N3) lies at  $-5.03$  eV and is centred on the NCS moiety where the donor group is situated, while the LUMO lies at  $-3.01$  eV and is centred on the 4,4-dicarboxy-2,2-bipyridine moiety where the acceptor group is situated. Upon absorption on a brookite cluster, the light absorption maximum red shifted to higher wavelength; this results in the distribution of the LUMO shifting from the dye to the TiO<sub>2</sub> cluster. The results suggest favourable electron injection from the dye excited state into TiO<sub>2</sub> semiconductor. The results suggest that TiO<sub>2</sub> brookite is a promising entrant for DSSC semiconductor.

**Keywords** Density functional theory · Dye sensitized solar cell · Ruthenium dye · Red shift on cluster formation · TiO<sub>2</sub> brookite

## 1 Introduction

In recent years, TiO<sub>2</sub> has been a subject of increasing interest due to its applications in pigments, photocatalysis and semiconductor materials in dye sensitized solar cells

---

I. F. Elegbeleye · N. E. Maluta

Department of Physics, University of Venda, Thohoyandou, South Africa

N. E. Maluta (✉) · R. R. Maphanga

National Institute for Theoretical Physics (NITheP), Gauteng, South Africa

e-mail: [Eric.Maluta@univen.ac.za](mailto:Eric.Maluta@univen.ac.za)

R. R. Maphanga

Council for Science and Industrial Research, P.O. Box 395, Pretoria, South Africa

© Springer Nature Switzerland AG 2020

L. Mammino et al. (eds.), *Advances in Quantum Systems in Chemistry, Physics, and Biology*, Progress in Theoretical Chemistry and Physics 32, [https://doi.org/10.1007/978-3-030-34941-7\\_8](https://doi.org/10.1007/978-3-030-34941-7_8)

(DSSCs) [1, 2]. The interest in  $\text{TiO}_2$  as semiconductor for dye sensitized solar cell is motivated by its non-toxicity and excellent stability upon illumination [1, 3–5]. However, the major drawback limiting its usage is its inability to absorb visible and infra-red photons of the solar spectrum because of its wide conduction band gap (3.0–3.2 eV) [5–7]. In DSSCs, dye molecules chemisorbed on the surface of  $\text{TiO}_2$  are used to harness light, and the consequent photoexcited electrons are injected into the conduction band of  $\text{TiO}_2$  [8–10]. An efficient photosensitizer must have good excited state properties and intense absorption in the visible and near infra-red region of the solar spectrum. Several dye molecules have been employed as sensitizer for DSSC; the highest efficiency in excess of 13% has been achieved in cells with nanostructured  $\text{TiO}_2$  semiconductor sensitized by Ruthenium (II) polypyridyl complex(N3) [11–15].

A significant number of studies has been done towards the surface modification of  $\text{TiO}_2$  crystals with atoms/sensitizing dye molecules to step-wise reduce the band gap and further enhance their activities in the visible and near infra-red region of the solar spectrum. Polymorphs of  $\text{TiO}_2$  have been a model for such studies, aimed at improving photocurrent yield and light harvesting in DSSCs [3, 16]. Energy band modulation by elemental doping, monodoping, codoping with nonmetals and transition metals, and adsorption of dye molecules on  $\text{TiO}_2$  surfaces, have been tested; the results showed improved spectral response and enhanced photocatalytic performances of  $\text{TiO}_2$  [7, 17]. Surfaces of rutile and anatase polymorphs have been greatly exploited and have been a prototypical model for basic studies on  $\text{TiO}_2$  oxide [18, 19]. Relatively limited work has been done on the brookite form of  $\text{TiO}_2$ , in contrast to rutile and anatase polymorphs that has been greatly exploited [4].

A recent study on  $\text{TiO}_2$  brookite suggested that it is a good photocatalyst and may exhibit higher photocatalytic activity than both rutile and anatase [4]. The absorption edge of brookite observed in a prior study was also reported to be broad and to extend to the visible region of the solar spectrum, in contrast to steep edges in the visible region observed for rutile and anatase polymorphs of  $\text{TiO}_2$  [19]. Since brookite surfaces have not been studied and are reported to have better photocatalytic properties, it is of keen interest to study the interactions of promising ruthenium (N3) dye molecules with surfaces of brookite  $\text{TiO}_2$  for optimization of photon current density in dye sensitized solar cells.

## 2 Computational Procedures

Optimization of the ground state geometries of the  $\text{TiO}_2$  brookite/ruthenium complex in the gas phase was performed using DFT with the hybrid B3LYP exchange correlation functional and the LANL2DZ pseudopotential for Ti atom; the 6–311+G (d, p) basis set was used for the C, N, O and H atoms. All DFT/TD-DFT calculations on the ruthenium (N3) complex were done using Gaussian 03 quantum chemical package [20]. The UV-Vis simulated absorption spectrum of the  $\text{TiO}_2$ /dye complex was computed by Time dependent (TD) DFT *in vacuo* with the same functional and basis set. 80 singlet to singlet electronic transitions were considered for the excitations,

to account for the whole absorption spectrum [21]. The UV-Vis spectra, maximum excitation wavelength, excitation energies, oscillator strength and light harvesting efficiency of the dyes were computed. Their matching with the solar spectrum is discussed. The light harvesting efficiency (LHE) at the maximum spectrum wavelength ( $\lambda_{\text{max}}$ ) was computed for the ruthenium (N3) complex using Eq. 1,

$$LHE = 1 - 10^{-f} \quad (1)$$

where “f” is the absorption strength of the dye associated with the maximum absorption of the dye (also called the oscillator strength) [15, 22, 23].

The absolute values of the adsorption energies of ruthenium (N3) complex on  $\text{TiO}_2$  were computed using Eq. 2.

$$E_{ads} = E_{dye} + E_{\text{TiO}_2} - (E_{dye+\text{TiO}_2}) \quad (2)$$

where  $E_{ads}$  is the adsorption energy,  $E_{dye}$  is the energy of the dye,  $E_{(\text{TiO}_2)}$  is the energy of the  $\text{TiO}_2$  slab and  $E_{(dye+\text{TiO}_2)}$  is the total energy of the dye- $\text{TiO}_2$  complex. A positive value of  $E_{ads}$  indicates stable adsorption [14, 24, 25].

The energies of the HOMO and LUMO, the HOMO-LUMO energy gap and the isodensity surfaces of the molecular orbitals involved in the excitation of the ruthenium (N3) complex were identified from the fchk file obtained from the simulations.

The bulk structure of brookite  $\text{TiO}_2$  that was used for this study was optimized using the CASTEP module in Materials Studio BIOVIA [26] to obtain the ground state structure of the  $\text{TiO}_2$  brookite semiconductor. The convergence energies and k-points were 650 eV and  $4 \times 7 \times 7$  respectively where k-points is the radius of convergence in the brillouin zone. The optimized structure of the ruthenium (N3) complex was exported into an atomic simulation environment via Avogadro Software [27]. DFT with the PBE functional was used through GPAW [28] and AVOGADRO [27] computational software within the atomic simulation environment to explore the optical properties of two modelled  $\text{TiO}_2$  brookite clusters, that is  $\text{Ti}_8\text{O}_{16}$  and  $\text{Ti}_{68}\text{O}_{136}$ . The optical properties of the interplay of ruthenium (N3) dye molecules with brookite  $\text{Ti}_8\text{O}_{16}$  and  $\text{Ti}_{68}\text{O}_{136}$  clusters were investigated using DFT, in order to optimize photon current densities in DSSCs.

### 3 Results and Discussions

#### 3.1 Geometric Properties of the Ruthenium (N3) Complex

The molecular structure of the ruthenium (N3) complex studied in this work is shown in Fig. 1 and its optimized geometry in Fig. 2. Figure 2 shows that the ruthenium atom is octahedral coordinated to six nitrogen atoms pertaining to the two thiocyanate

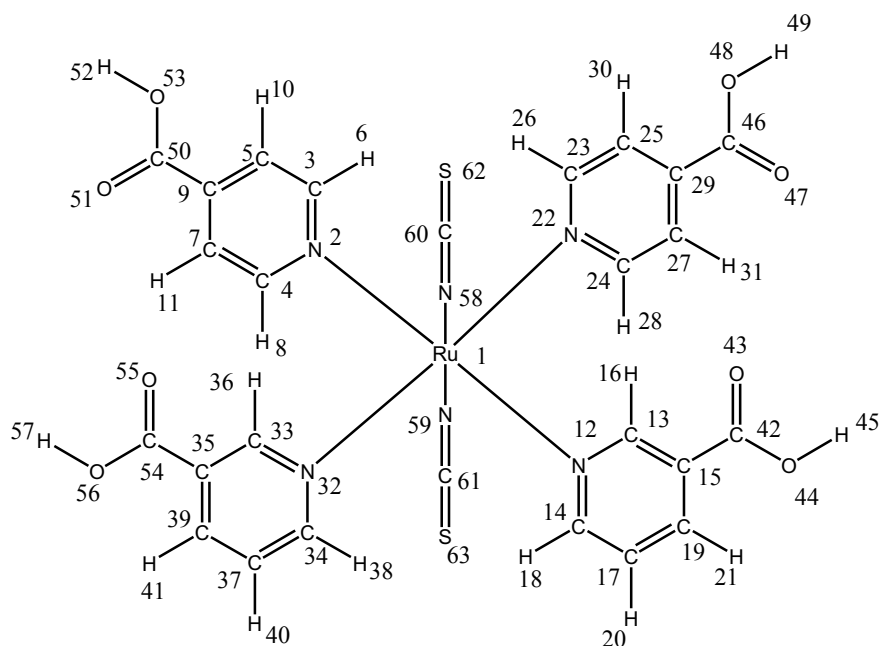


**Fig. 1** Molecular structure of ruthenium (N3) complex and atom numbering utilized in this work

and the four carboxylic acids of the two bipyridyl ligands. Selected bond lengths and bond angles of the optimized geometry of the ruthenium (N3) complex are reported in Table 1. The geometry optimization of ruthenium (N3) complex converged when the internal forces acting on all the atoms were less than  $4.9 \times 10^{-5}$  eV and a threshold value of  $4.5 \times 10^{-4}$  eV/atom. The dipole moments obtained after optimization is 2.8633.

### 3.2 UV/VIS Absorption Spectrum of the Calculated Ruthenium (N3) Complex

As already mentioned, 80 singlets to singlet transitions were considered for this complex in order to account for the whole spectrum. The absorption spectrum in gas phase is presented in Fig. 3. The ruthenium sensitizer shows good absorption in the UV and visible region of the solar spectrum with intense absorption around 311 nm, 388 nm and 480 nm, but the peak ( $\lambda_{\max}$ ) is more notable at 480 nm. This calculated  $\lambda_{\max}$  peak of the ruthenium (N3) sensitizer is in close agreement with experimental and computed values reported in literature [23, 29]. Hence, the DFT/B3LYP level of theory with the selected basis set can be considered adequate for the simulation of the absorption spectra of the ruthenium (N3) complex dye.

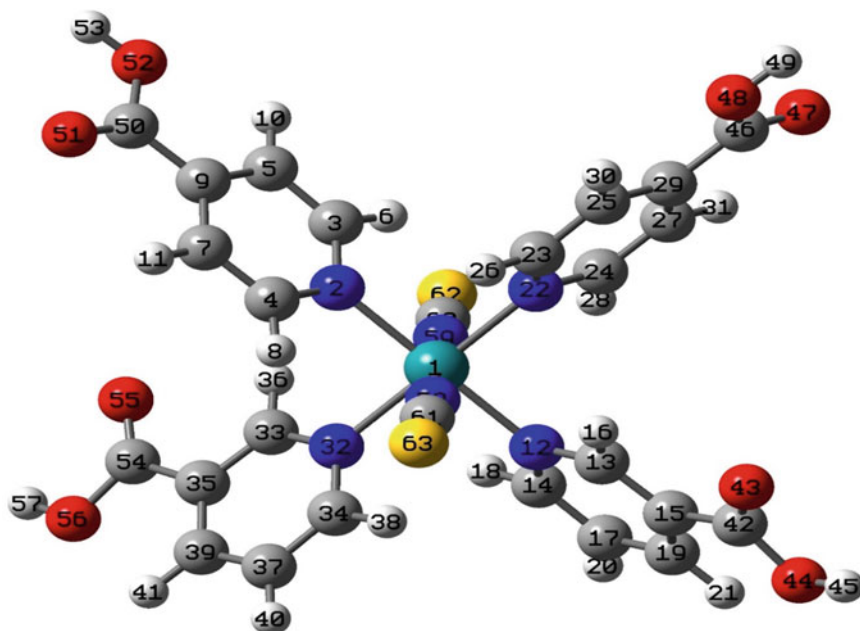


**Fig. 2** Optimized geometry of the ruthenium (N3) complex ([cis-di (thiocyanate) bis (2,2'-bipyridine-4,4'-dicarboxylate) ruthenium]) Ru(dcbpy)(NCS)<sub>2</sub> and colours of atoms utilized in this work (Olive green for ruthenium atoms, blue for nitrogen atoms, yellow for sulphur atoms, grey for carbon atoms and red for oxygen atoms)

**Table 1** Selected bond lengths (Å) and bond angles (degrees) of ruthenium (N3) complex

Bond length (Å)		Bond angles (°)	
Length considered	Value of length	Angles considered	Value of angles
Ru-N2	2.096	N2-Ru-N12	89.8
Ru-N12	2.109	N2-Ru-N12	89.8
Ru-N22	2.096	N32-Ru-N59	89.8
Ru-N32	2.109	N12-Ru-N59	89.2
Ru-N58	2.065	N32-Ru-N12	90.3
Ru-N59	2.065	N58-Ru-12	89.8

### 3.2.1 Light Harvesting Efficiency of Ruthenium (N3) Complex

The light harvesting efficiencies of the dye molecules were calculated theoretically using Eq. 1.

The highest oscillator strength of the ruthenium (N3) complex is 0.15, yielding a corresponding calculated light harvesting efficiency of 0.29 (Table 2). Considering

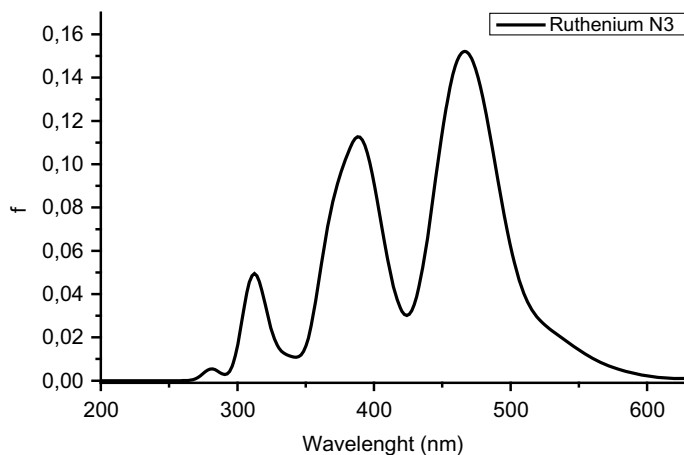


**Fig. 3** Simulated absorption spectra (oscillator strength,  $f$ , versus wavelength) of ruthenium (N3) complex

**Table 2** Computed light harvesting efficiencies of ruthenium (N3) complex at the three absorption peaks

Wavelength (nm)	Oscillator strength	LHE	LHE (%)	Wavelength (nm)
311	0.05	0.10	10	311
388	0.11	0.22	22	388
480	0.15	0.29	29	480

all the three absorption peaks, the ruthenium complex has an average LHE value of 20.1%.

### 3.2.2 The Computed Energies of HOMO and LUMO, HOMO-LUMO Energy Gap and Isodensity Surfaces of Ruthenium (N3) Complex

The computed energies of HOMO and LUMO and the HOMO-LUMO energy gap of the ruthenium (N3) complex are presented in Table 3 and compared with the results of

**Table 3** Energies of HOMO, LUMO and HOMO-LUMO energy gap of the ruthenium (N3) complex

Dye (N3)	HOMO (eV)	LUMO (eV)	H-L gap (eV)
Experimental work [24, 29]	-5.36	-3.47	1.89
Computed [23]	-5.67	-3.63	1.96
This work	-5.03	-3.01	2.02

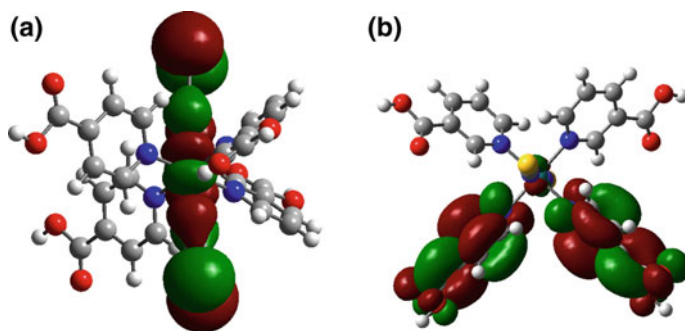


**Fig. 4** Isodensity surfaces of ruthenium (N3) complex **a** HOMO **b** LUMO. Isovalue = 0.02

another works [23, 26], and with the experimental values [29]. The reported experimental values of the energies of the HOMO, LUMO and HOMO-LUMO energy gap of the ruthenium (N3) complex are  $-5.36$  eV,  $-3.47$  eV and  $1.89$  respectively. The results obtained in this work compares favourably with the simulated and experimental result [23, 26, 29].

The isodensity surfaces of the HOMO and LUMO of the ruthenium (N3) complex are presented in Fig. 4. The HOMO is distributed on the thiocyanate ligands, while the LUMO is distributed on the two dc bpy 4,4-dicarboxy-2,2-bipyridine ligands. The different distributions of the HOMO and LUMO indicates good electron injection properties of the ruthenium (N3) complex, due to various donor and acceptor levels.

### 3.3 Adsorption of Ruthenium (N3) Complex Dye on Brookite $\text{TiO}_2$ Nanocluster

The brookite clusters studied in this work are  $(\text{TiO}_2)_n$  with  $n = 8$  and  $n = 68$ . Figure 5 shows the brookite  $(\text{TiO}_2)_8$  model comprises of eight titanium and sixteen oxygen atoms, the structure of brookite  $(\text{TiO}_2)_8$  was imported from CASTEP materials studio [29] via the crystallographic mode (cif) without periodicity into Avogadro visualizing interface. Figure 6 reveals a periodic brookite  $(\text{TiO}_2)_{68}$  supercell  $2 \times 2 \times 2 \text{ \AA}$  comprising of sixty-eight titanium atoms and one hundred and thirty six oxygen atom. The ruthenium (N3) dye molecules were adsorbed on  $(\text{TiO}_2)_8$  and  $(\text{TiO}_2)_{68}$  brookite cluster by bidentate adsorption mode in which each of the oxygen of the carboxylic group binds to a two-fold coordinated and four-fold coordinated titanium atom on  $(\text{TiO}_2)_8$  and  $(\text{TiO}_2)_{68}$  brookite cluster, as shown in Fig. 7. This adsorption mode was found to be the most energetically favourable, especially for ruthenium complexes with two bipyridine ligands having carboxylic acid functional groups. The results were presented on relaxation energies, optical excitation spectrum and isodensity surfaces of the key molecular orbital involved in excitation.

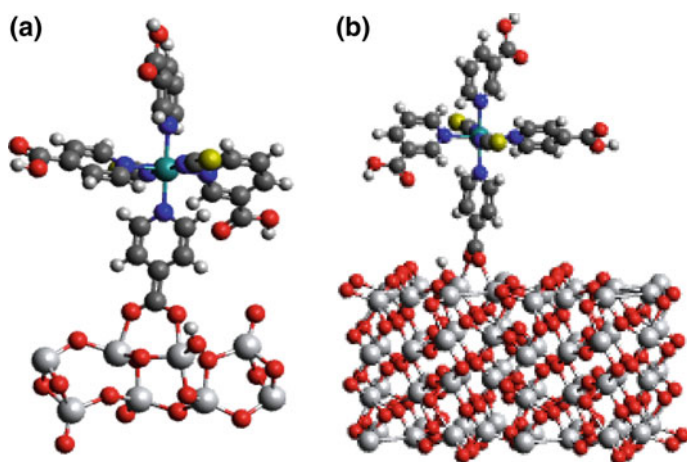


**Fig. 5** Ruthenium (N3) complex absorbed on **a**  $(\text{TiO}_2)_8$  brookite cluster **b**  $(\text{TiO}_2)_{68}$  brookite cluster

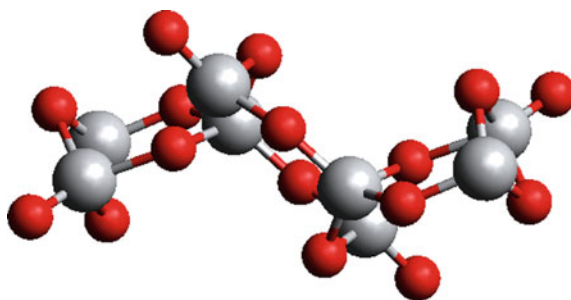


**Fig. 6**  $(\text{TiO}_2)_8$  brookite cluster

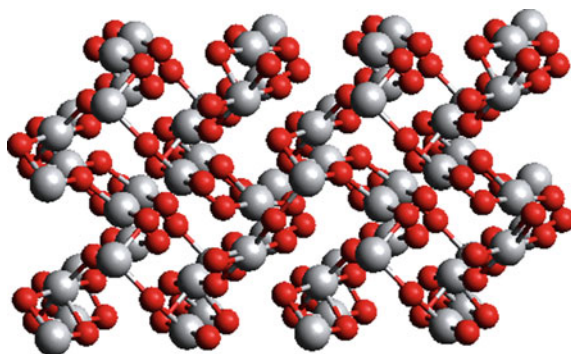


**Fig. 7**  $(\text{TiO}_2)_{68}$  brookite supercell



**Table 4** Relaxation energies of ruthenium (N3) dye molecule absorbed on  $(\text{TiO}_2)_8$  and  $(\text{TiO}_2)_{68}$  brookite cluster

System	Relaxation energy (eV)	Energy $(\text{TiO}_2)_n$ cluster (slab) (eV)	Energy <sub>(slab +molecule) Dyes@<math>(\text{TiO}_2)_n</math></sub> (eV)
Ruthenium (N3)	-432.919		
$(\text{TiO}_2)_8$		-198.308	
$(\text{TiO}_2)_{68}$		-1635.558	
Ruthenium@ $(\text{TiO}_2)_8$			-632.953
Ruthenium@ $(\text{TiO}_2)_{68}$			-2072.267

### 3.4 Adsorption Energies of Ruthenium (N3) Dye Molecule Absorbed on $(\text{TiO}_2)_n$ , $n = 8, 68$ Brookite Complex

The relaxation energy for ruthenium (N3) dye is  $-432.91$  eV. The energy of the clusters are  $-198.31$  eV,  $-1635.55$  eV for  $(\text{TiO}_2)_8$  and  $(\text{TiO}_2)_{68}$  respectively (Table 4). The adsorption energies of ruthenium (N3) dye on  $(\text{TiO}_2)_8$  and  $(\text{TiO}_2)_{68}$  brookite cluster were computed using Eq. 2.

The adsorption energy of ruthenium (N3) dye @  $(\text{TiO}_2)_8$  is  $1.73$  eV and of ruthenium (N3) dye @  $(\text{TiO}_2)_{68}$  is  $3.76$  eV. These positive adsorption energies denote the ability of the dye molecules to bind to the surface of  $(\text{TiO}_2)_8$  and  $(\text{TiO}_2)_{68}$  clusters. The adsorption energy of ruthenium (N3) dye on  $(\text{TiO}_2)_{68}$  and  $(\text{TiO}_2)_8$  brookite cluster are  $3.84$  eV and  $1.73$  eV respectively. The results shows that the ruthenium (N3) dye binds more strongly to the surface of the larger cluster  $(\text{TiO}_2)_{68}$  brookite than the corresponding  $(\text{TiO}_2)_8$  brookite cluster.

#### 3.4.1 Absorption Spectrum of Ruthenium (N3) Dyes Absorbed on $(\text{TiO}_2)_8$ and $(\text{TiO}_2)_{68}$ Brookite Cluster

The optical spectra of the ruthenium (N3) dye absorbed on  $(\text{TiO}_2)_8$  is presented in Fig. 8, in which the absorption corresponds to the optical excitation of the ruthenium (N3) dye absorbed on  $(\text{TiO}_2)_8$ . Comparing the absorption spectra of the  $(\text{TiO}_2)_8$  cluster (Fig. 8) with the absorption spectra of the ruthenium (N3) dye absorbed on the  $(\text{TiO}_2)_8$  cluster (Fig. 9), shows that the absorption spectra of  $(\text{TiO}_2)_8$  cluster shows excitation in the UV region around  $200$ – $400$  nm, while the absorption spectra of the ruthenium@  $(\text{TiO}_2)_8$  shows absorption in the visible region around  $400$ – $600$  nm, with a near infra-red region where a maximum occur around  $1100$  nm. The results suggest that the absorption of the ruthenium (N3) dye on  $(\text{TiO}_2)_8$  brookite gives rise to a bathochromatic shift of the absorption maxima to higher wavelengths. Furthermore, absorption is observed over a wide range from the visible to the far infrared regions. The red shift observed upon absorption on ruthenium (N3) dye on  $(\text{TiO}_2)_8$  brookite clusters suggests good optical properties of the ruthenium (N3) dye molecules and agrees with earlier reports on the good photocatalytic properties of brookite  $\text{TiO}_2$  [17, 30, 31].

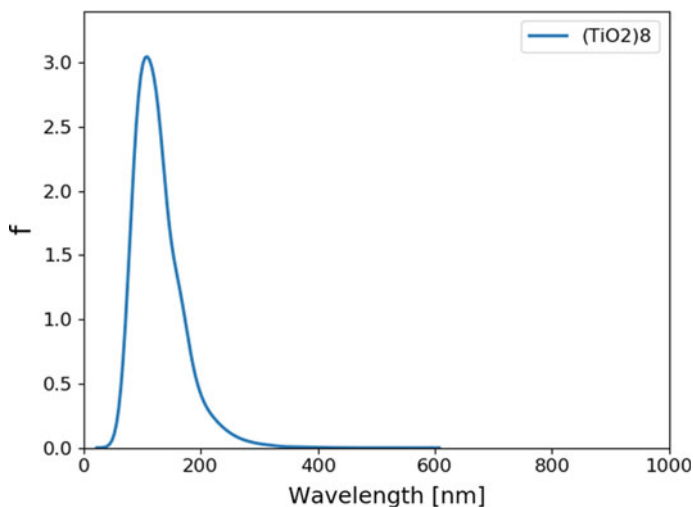


**Fig. 8** UV/Vis absorption spectrum (oscillator strength,  $f$ , versus wavelength) of  $(\text{TiO}_2)_8$  brookite cluster

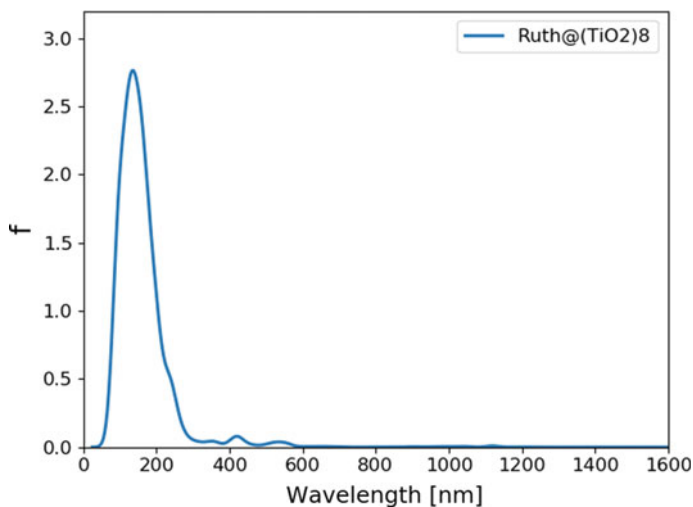


**Fig. 9** UV/Vis absorption spectrum (oscillator strength,  $f$ , versus wavelength) of ruthenium (N3) complex absorbed on  $(\text{TiO}_2)_8$  brookite cluster

### 3.4.2 Isodensity Surfaces of the Ruthenium (N3) Dye Absorbed on $(\text{TiO}_2)_n$ , $n = 8, 68$ Brookite Cluster

The isodensity surfaces of the frontier molecular orbitals (HOMO and LUMO) involved in the photoexcitation of the ruthenium (N3) complex absorbed on  $(\text{TiO}_2)_8$

and  $(\text{TiO}_2)_{68}$  clusters are shown in Figs. 10 and 11 respectively. The results show that the HOMO is mainly concentrated on the dye donor group where the occupied electronic orbitals are located, while the LUMO is distributed over the  $\text{TiO}_2$ . The distribution of the LUMO very close to the surface of  $\text{TiO}_2$  is due to the nature of the ruthenium dye and also suggest that the dyes are energetically in proximity to bind to the surface of  $\text{TiO}_2$  upon adsorption, the position of the LUMO agrees with other literature report on ruthenium N3 complex [32]. This suggests electron transfer between the occupied excited state of the dye and the unoccupied acceptor levels of the semiconductor conduction band. The localization of the HOMO electronic level

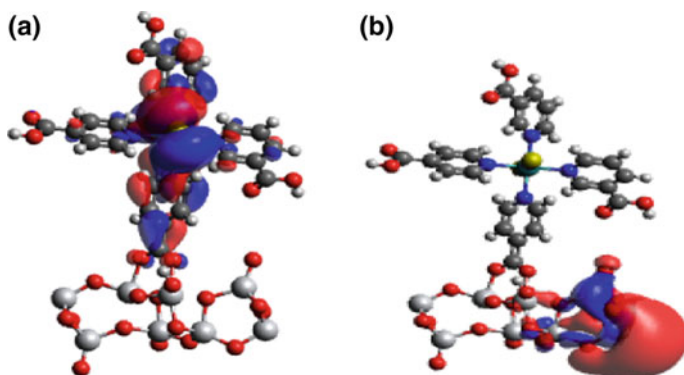


**Fig. 10** Isodensity surfaces of **a** HOMO of ruthenium (N3) @  $(\text{TiO}_2)_8$  **b** LUMO of ruthenium (N3) @  $(\text{TiO}_2)_8$  brookite cluster

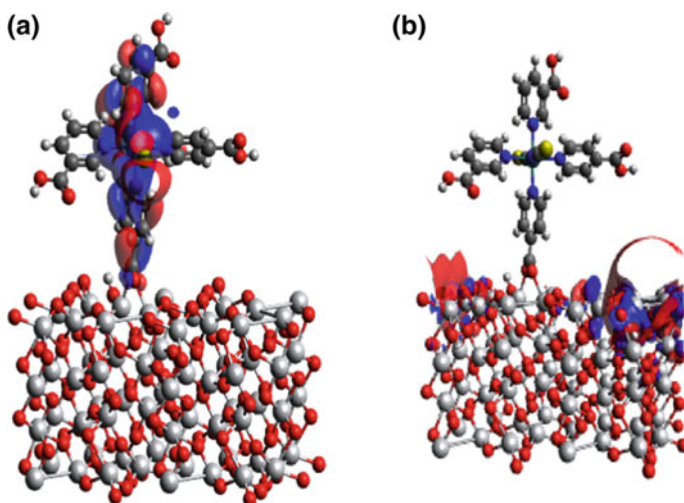


**Fig. 11** Isodensity surfaces of **a** HOMO of ruthenium (N3) @  $(\text{TiO}_2)_{68}$  brookite cluster **b** LUMO of ruthenium (N3) @  $(\text{TiO}_2)_{68}$  brookite cluster

on the dye molecules and the LUMO electronic level on the TiO<sub>2</sub> clusters in Figs. 10 and 11 implies efficient separation of charge upon adsorption and electron injection from the dye excited state into the TiO<sub>2</sub> semiconductor conduction band.

## 4 Conclusions

A DFT study of a ruthenium (N3) complex was performed successfully for application in dye sensitized solar cells. The optical absorption, UV-Vis spectrum and light harvesting efficiency of the dye molecule were investigated. The results show that the light harvesting efficiency depends on the absorption strength of the dyes. The absorption of the ruthenium (N3) complex on the TiO<sub>2</sub> brookite semiconductors showed that the dye has a stable grafting to the surface of TiO<sub>2</sub>. A red shifting of the absorption maxima to the near infra-red region also suggests good optical properties of the dye and the brookite polymorph. The location of the HOMO and LUMO which is visible on the isodensity surfaces of the dye-TiO<sub>2</sub> implies efficient separation of charges upon adsorption and electron injection from the dye excited state into the TiO<sub>2</sub> semiconductor conduction band. Our findings generally suggest that the ruthenium (N3) complex dye molecule and brookite semiconductors exhibit promising features for application in DSSCs.

## References

1. Beltran A, Gracia L, Andres J (2006) *J Phys Chem B* 110:23417–23423
2. Tong Z, Shang PG (2014) *Amer Chem Soc* 118:11385–11396
3. Hao Y, Jia L, Gang Z, Sum WC, Hongda D, Lin G, Chengjun FK, Wenhui D (2015) *Roy Soc Chem Advan* 5:60230–60236
4. Monique MR, Xihong P, Lianjun L, Ying L, Jean MA (2012) *J Phys Chem* 116:19755–19764
5. Yaqin W, Ruirui Z, Jianbao L, Liangliang L, Shiwei L (2014) *Nano Res Lett* 9:1–8
6. Jun Z, Lisha Q, Wei F, Junhua X, Zhenguo J (2014) *Amer Cer Soc* 97:2615–2622
7. Hou XG, Huang M, Wu XL, Liu A (2009) *Science Chin Ser G-Phys Mech Astr* 52:838–842
8. Mohammad NK, De Angelis F, Fantacci S, Selloni A, Viscardi G, Liska P, Ito S, Bessho M, Gratzel T (2005) *J Amer Chem Soc* 127:16835–16846
9. Jinxia L, Chun Z, Zexing C (2013) *Phys Chem Chem Phys* 15:13844–13851
10. Chiara A, Edoardo M, Mariachiara P, Enrico R, Fillipo A (2012) *Phys Chem Chem Phys* 14:15963–15974
11. Yella A, Lee HW, Tsao HN, Yi C, Chandiran AK, Nazeeruddin MK, Diao EWG, Yeh CY, Zakeeruddin SM, Gratzel M (2011). *Sci* 334, 629–634
12. Cai RZ, Zi Jiang L, Yu HC, Hong SC, You ZW, Wang JF, Dao BW (2010) *DFT Curr Appl Phys* 10:77–83
13. Jungsuttiwong S, Tarsang R, Pansay S, Yakhantip T, Promarak V, Sudyoasudk T, Kaewin T, Saengsuwan S, Namuangrak S (1999) *Int J Chem Mol Nuc Mater and Metallur Eng* 77:561–567
14. Avinnash P, Ramesh KCH, Bhanuprakash K (2012) *J Chem Sci* 124:301–310
15. Ramesh KC, Manho L, Xingfa G, Joonkyung J (2015) *J Mol Mod* 21(297):1–8
16. Barbara V, Folarin W, Thomas B, Dominic L (2012) *ACS PubAmer Chem Soc* 28:11354–11363

17. Schaub R, Wahlstrom E, Ronnau A, Laegsgaard E, Stensgaard I, Besenbacher F (2003) *Sci*, 299:377–379
18. Ken O, Bin L, Jin Z, Kenneth DJ, Jinlong Y, Hrvoje P (2005) *Sci* 308:1154–1158
19. Zallen R, Moret MP (2006) *Sol Stat Comm* 137:154–157
20. Frisch MJ, Trucks GW, Schlegel HB, Scuseria GE, Robb MA, Cheeseman JR, Montgomery JA, Jr Vreven T, Kudin KN, Burant JC, Millam JM, Iyengar SS, Tomasi J, Barone V, Mennucci B, Cossi M, Scalmani G, Rega N, Petersson GA, Nakatsuji H, Hada M, Ehara M, Toyota K, Fukuda R, Hasegawa J, Ishida M, Nakajima T, Honda Y, Kitao O, Nakai H, Klene M, Li X, Knox JE, Hratchian HP, Cross JB, Adamo C, Jaramillo J, Gomperts R, Stratmann RE, Yazyev O, Austin AJ, Cammi R, Pomelli C, Ochterski JW, Ayala PY, Morokuma K, Voth GA, Salvador P, Dannenberg JJ, Zakrzewski VG, Dapprich S, Daniels AD, Strain MC, Farkas O, Malick DK, Rabuck AD, Raghavachari K, Foresman JB, Ortiz JV, Cui Q, Baboul AG, Clifford S, Cioslowski J, Stefanov BB, Liu G, Liashenko A, Piskorz P, Komaromi I, Martin RL, Fox DJ, Keith T, Al-Laham MA, Peng CY, Nanayakkara A, Challacombe M, Gill PMW, Johnson B, Chen W, Wong MW, Gonzalez C, Pople JA (2004) *Gaussian 03*, revision D.01. Gaussian, Inc., Wallingford, CT
21. Corneliu I, Opre PP, Fanica C, Marilena F, Mihai AG (2013) *Mat* 6:2372–2392
22. Asif M, Salah UK, Usman AR, Mudassir HT (2014) *Arab J Chem* 1–7
23. Umer M, Ibelwaleed A, Hussein KH, Shakeel A (2015) *J Advan Mater Sci Eng* 2015:1–8
24. Emildo M (2017) *Phys Sci Rev* 6:1–9
25. Prajongtat P, Suramit S, Nokbin S, Nakajima K, Misuke K, Hannongbua S (2017) *J mol Graph and Model* 76:551–561
26. Clark SJ, Segall MD, Pickard CJ, Hasnip PJ, Probert MJ, Refson K, Yates JR, Payne MC (2005) 220:576–570
27. Hanwell MD, Curtis DE, Lonie DC, Vandermeersch T, Zurek E, Hutchison GR (2012) *J Cheminform* 4
28. Mortensen JJ, Hansen LB, Jacobsen KW (2005) *Phys Rev B* 71:1–11
29. Anthonysamy A, Lee Y, Karunakaran B (2015) *J Mat Chem* 21:12389–12397
30. Agatino DP, Marianna B, Leonardo P (2013) *Cat* 3:36–73
31. Gong X, Selloni A (2007) *Phys Rev B* 76:235307
32. Ramesh KC, Joonkyung J (2018) *Sol Ener* 383–290